MAPAN-JOURNAL ,
Publisher: METROLOGY SOC INDIA , NPL PREMISES,
Address: DR K S KRISHNAN MARG, NEW DELHI, INDIA,
ISSN / eISSN:0970-3950 / 0974-9853
Volume 25-Issue 1-(2025)
https://doi-001.org/1025/17637108315396

Stability Study of Photovoltaic Tracking Mounts under High Wind Conditions

Chi Zhang1 , Xiaojun Xue2 , Lei Li3 , Bo Zhu4 , Liang Lu5 , Juewei Wang6 ,

Xianglong Hou7 , Jinliang Yan*

Dongfang Electric Corporation International Cooperation Co., Ltd., 611731, China

1Email：zhangchi@dongfang.com.cn

corresponding author：**yanjinliang@dongfang.com.cn**

（Author, Affiliation）

Summary：Photovoltaic tracking brackets have been widely used in large-scale photovoltaic power plants due to their excellent power generation gain. However, the stability of their structure under high wind conditions is becoming increasingly prominent, becoming one of the key factors restricting their widespread application. This paper addresses the stability problem of photovoltaic tracking brackets under high wind speeds by conducting a systematic study using a combination of theoretical calculations, finite element analysis, and load testing. Wind load models were established based on standards such as AISC360 and ASCE. The stress distribution of the bracket structure under extreme wind conditions was simulated using ANSYS finite element software, and wind tunnel experiments and multi-condition physical tests were conducted using a 1:20 scale model. The results show that under an extreme wind speed of 49 m/s, the maximum tensile stress of the M20-8.8 bolts is 28.1 MPa, with a strength utilization rate of 0.062, and the combined stress of the U-shaped bearing seat is 196 MPa, with a utilization rate of 0.552, both meeting the standard requirements. Torsional physical tests show that the failure threshold reaches 18.4 kN·m. To address the stability issues involved in this environment, this paper optimizes the purlin structure, establishing finite element models of purlin structures with and without diagonal bracing, and analyzing their buckling instability response under both upward and downward pressure conditions. The study shows that optimizing the purlin thickness, the position and length of the U-shaped reinforcement, and the arrangement angle and thickness of the diagonal bracing can significantly improve the critical load for purlin instability. Among these optimizations, placing the U-shaped reinforcement within a 50-70mm radius of the purlin center is particularly effective in improving

structural stability. Compared to increasing yield strength by replacing the material with high-strength Q500 steel, optimizing the structural form has greater practical value in suppressing local buckling.

Keywords：Photovoltaic tracking brackets; high wind stability; wind load model; finite element analysis; physical testing

1 introduction

As the photovoltaic industry develops towards high efficiency and intelligence, tracking brackets are widely used because they can increase power generation by 15%~25% [1]. However, extreme winds (≥30m/s) have become the main cause of tracking bracket failure. According to statistics, from 2020 to 2024, the proportion of bracket damage caused by wind disasters in domestic photovoltaic power plants reached 47% [2]. As one of the mainstream types, the cantilever structure of the single-axis horizontal tracking bracket is susceptible to the coupling effect of overturning moment and bending stress in strong winds, and there are risks such as shaft breakage, foundation slippage, and component detachment [3]. At present, domestic and foreign research mainly focuses on wind load theoretical calculation and structural optimization. The IEC 61215 standard gives the recommended value of the wind load shape coefficient of photovoltaic modules, but does not consider the influence of the tracking angle on the overall wind effect of the bracket [4]. Zhang Yifan [5] analyzed the wind resistance coefficient of brackets with different tilt angles through CFD simulation, but lacks experimental verification. Chen Xiaoqiang [6] proposed a lightweight design method for brackets based on genetic algorithm, but did not solve the stability problem under extreme working conditions. In order to better solve this problem, researchers have explored the optimization of purlin structures in recent years to address the stability problem under this condition [7, 8]. One type of research focuses on the material level, attempting to delay the buckling or failure time by increasing the yield strength of purlin steel. For example, Liang et al. [9] and Wang Weiyong et al. [10] improved the stability of components by using high-strength steel, but their research showed that under the condition of thin-walled purlins with a high slenderness ratio, buckling still occurs before yielding, and the improvement of the structure's resistance to instability is limited. In addition, the poor weldability and high cost of high-strength steel also limit its application in large-scale photovoltaic projects. Another type of research starts from the optimization of structural form, improving the overall stability by improving the geometric parameters of components and strengthening local stiffness. Methods such as improving the cross-sectional shape of purlins [11], setting web openings for reinforcement [12], and optimizing the purlin arrangement spacing and

support method [13] can all improve the stress path and stress distribution without significantly increasing costs. Among them, diagonal bracing and U-shaped reinforcement are effective means to suppress local buckling of thin-walled members and have been gradually adopted in the design of steel structure nodes, cold-formed members and photovoltaic brackets[14]. However, most of the existing studies are based on simplified working conditions or local member analysis, and there is still a lack of systematic optimization strategies and response laws for the complete purlin system under the coupled upper and lower pressure conditions. In addition, in terms of structural optimization methods, finite element modeling and parameter sensitivity analysis have become important tools for the current structural anti-instability design. Přemys et al.[15] used nonlinear finite element simulation to systematically analyze the buckling behavior of cold-formed members under different loading paths, providing technical means for multi-parameter structural optimization. However, how to unify the material properties, structural parameter thickness, reinforcement size, diagonal bracing angle and actual photovoltaic bracket construction requirements is still an important challenge. In particular, for the hybrid support mode with/without diagonal bracing, its buckling control mechanism is still unclear and there is a lack of a unified structural configuration evaluation system. Although existing studies have made progress in their respective fields, there is still room for improvement in multi-factor coupling analysis and practical engineering applications. Traditional design methods often rely on static load assumptions, failing to adequately consider the coupling effect of turbulent pulsating wind and structural vibration, leading to insufficient wind-resistant safety redundancy in actual engineering projects. This paper, based on a 310MW demonstration project and in accordance with standards such as AISC360 and ASCE7-16, systematically studies the mechanical response of the tracking support under extreme wind conditions using multi-scale analysis methods. The focus is on addressing the nonlinear relationship between wind load and structural response, as well as the dynamic mechanical characteristics of bolted connections. Simultaneously, this study constructs a complete finite element model of the photovoltaic purlin system, covering dual stability analysis under typical wind and snow load conditions. A systematic structural optimization process is proposed, effectively delaying local buckling failure modes through multi-parameter control. The coupled influence of material strength and structural form on stability is quantitatively evaluated, providing a reliable engineering reference for photovoltaic purlin design. Based on this, in terms of structural arrangement, this paper introduces finite element modeling methods and boundary condition settings, conducting optimization analyses of thickness, reinforcement, and brace angles for structures with and without diagonal braces, and comparing and evaluating different optimization schemes and material options.

。

2 Comprehensive Study on Stability of Supports under High Wind

Conditions

2.1 Photovoltaic tracking bracket selection calculation and load model

2.1.1 Support structure

The single-axis photovoltaic tracking bracket described in this article is a spatial beam frame structure, mainly composed of columns, swing arms, push rods, main beams, and secondary beams (purlins). The upper end of the column is connected to a bearing seat via a column joint. The bearing seat and bearing cover cooperate to hold the main beam, enabling the main beam to rotate. The swing arm is fixed to the main beam, with one end connected to the push rod, the other end of which is fixed to the lower end of the column. When the push rod operates, the working condition of the main beam is adjusted by changing the angle of the swing arm. The photovoltaic modules are installed on the purlins, which are fixed to the main beam. Ultimately, the main beam drives the photovoltaic modules to rotate around their axis, achieving tilt angle adjustment. Its structural diagram is shown in Figure 1.

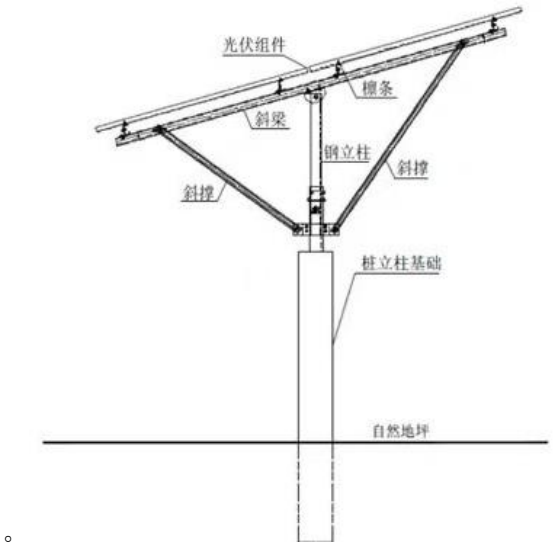

。

Figure 1. Cantilevered single-axis horizontal tracking bracket

2.1.2 Wind load model construction

Under high wind conditions, the main external force on the tracking support is wind load, and its calculation needs to consider factors such as wind speed, wind direction, windward area, component tilt angle, and aerodynamic coefficient. The wind load formula defined in my country's building structure design code is as follows:

$$F_w = \frac{1}{2} \cdot \rho \cdot C_d(\theta) \cdot A \cdot V^2 \qquad (1)$$

In the formula, Fw is the wind load per unit area (N/m2); ρ is the air density, typically taken as

1.225 kg/m2; Cd(θ) is the wind pressure coefficient, which depends on the component tilt angle θ; A is the windward area; and V is the wind speed. To improve the model accuracy, this study introduces a table of wind pressure coefficients corresponding to different tilt angles and considers the special wind load distribution characteristics of the tracking system at the extreme angle (±60°). Furthermore, the wind vibration effect is simplified and corrected to estimate the impact of periodic wind force on structural stability.

2.1.3 Structural mechanics model establishment

A nonlinear mechanical model considering bolt preload is established for the connection between the rotary drive and the column. Taking an M20-8.8 bolt (Fu=800MPa) as an example, the combined stress of axial tensile force T and shear force V is calculated as follows:

:

$$f_{rt} = \frac{T}{A_b} \quad (2)$$

$$f_{rv} = \frac{V}{A_b} \quad (3)$$

In the formula, Ab is the cross-sectional area of the bolt, T represents the axial tensile force borne by the bolt, and V represents the shear force.

2.1.4 Finite element analysis

This study used ANSYS Workbench 2022 R1 to build a 3D solid model. The main support structure is made of Q355 steel with an elastic modulus E = 210 GPa, Poisson's ratio ν = 0.3, and yield strength Fy = 355 MPa. The bolts are made of 8.8 grade high-strength steel with a tensile strength Fu = 800 MPa and a yield strength σy = 640 MPa. The bearing housing is made of Q355B steel with a thickness t = 12 mm. The loading conditions are shown in Table 1.

A hexahedral dominant mesh was used. Sweep meshing was used for bolt holes and corner welds in critical areas, with the element size controlled within 5 mm. The mesh size for ordinary areas was 10 mm. The total number of elements was approximately 245,000, and the number of nodes was approximately 387,000. The stress error was verified to be ≤3% through mesh independence. The rotary drive connection surface was set to "Fixed Support," with Ux = Uy = Uz = 0, simulating a completely fixed constraint in the field. The bottom of the bearing housing was set to "Cylindrical Support," allowing axial rotation but restricting radial displacement. The loading conditions are shown in the table. The equivalent stress von Mises stress contour plot was extracted, focusing on areas such as the area around the bolt holes and the web of the bearing housing.

Table 1 Loading Conditions

Operating condition number	TorqueM	Compression*Nc*	Horizontal force*V*	pull*NT*	Simulated scenario
Operating conditions 1	5.9 kN·m	27.4 kN	-	-	Pressure load under extreme wind conditions
Operating conditions 2	-	-	6.9 kN	25.5 kN	Horizontal wind load under operating conditions
Operating conditions 3	8.1 kN·m	-	-	1.8 kN	Corner bracket torsional combined load

2.2 Wind tunnel testing

2.2.1 Experimental Objectives and Methods

To verify the accuracy of the wind load model and further obtain the aerodynamic characteristics of the photovoltaic tracking bracket under different attitudes and wind angles, a small-scale model wind tunnel test was conducted. The experimental objectives included: obtaining the wind pressure coefficient at different component tilt angles; analyzing the impact of wind speed changes on the stress on various parts of the structure; exploring the impact of wind angle changes on the stability of the bracket system; and providing experimental basis for subsequent numerical simulation and engineering optimization.

This study uses a 1:20 scale model, with 8.8 grade M1.0 microbolts used for the bolt matching, achieving an equivalent strength ratio of 1:1. The bearing housing thickness was taken as 0.6 mm according to the scale. The component surface was coated with matte paint to reduce the influence of wind tunnel wall reflections.

2.2.2 Experimental setup and measurement scheme

Miniature pressure sensors (accuracy ±0.5Pa) were attached to the surface of photovoltaic modules and corners of the support structure to collect wind pressure distribution data. A six-component balance was installed on the support base to measure the overall aerodynamic forces, mainly lift, drag, and torque, with an accuracy of ±0.1% FS. Strain gauges were placed at bolt connections, U-shaped supports, and other key nodes to monitor stress concentration areas. First, the model was calibrated under no-load conditions with a wind speed of 5 m/s to verify that the balance zero-point drift was ≤0.05% FS. Then, graded loading was performed, with each load

condition increasing by 20%, 50%, 80%, and 100% of the target wind speed. Data was collected after each wind speed point stabilized for 30 seconds. Finally, a reverse limit test was conducted, gradually increasing the wind speed until model failure, recording the wind speed, stress distribution, and deformation mode at failure. The simulated conditions are shown in Table 2.

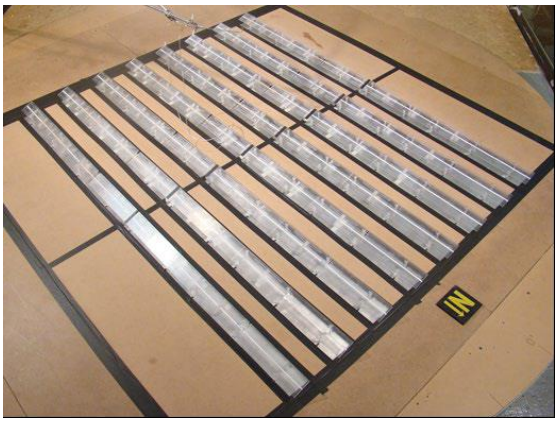

Figure 2 Wind tunnel pressure test

Table 2 Loading Conditions

Operating conditions	wind speed（m/s）	wind direction（°）	Turbulence intensity（%）	Simulated scenario
Operating conditions - Upward airflow	20	60	5	Normal operation upward wind load
Extreme operating conditions – down comer	49	0	10	Typhoon downforce
Cornering Conditions - Twisting Wind	30	10	8	Corner support torsional wind load

2.2.3 Wind Pressure Coefficient Distribution Characteristics

Experiments showed that under a 60° wind direction angle and a wind speed of 20 m/s, the average wind pressure coefficient on the upper surface of the module at a tilt angle of 15° was -2.04, a decrease of 24.4% compared to the 0° tilt angle (-1.64). Under extreme conditions with a wind speed of 49 m/s and a 0° wind direction, the module's downward wind pressure coefficient was 0.436, corresponding to a local wind pressure of 1088 Pa, with an error of only 3.7% compared to the Bernoulli equation calculation (theoretical value 1129 Pa). When the wind direction increased from 0° to 60°, the upward wind load coefficient of the module increased from GCN1uptwist = -0.8 to -2.04, resulting in an increase in the corner support torque from 5.5 kN·m to 8.3 kN·m

and the bolt axial tensile force from 8.8 kN to 13.2 kN, consistent with the theoretical calculation trend.

At a wind speed of 20 m/s and a wind direction of 60°, the lift FL = 12.5 kN, drag FD = 8.7 kN, and torque M = 5.9 kN·m measured by a six-component balance, which is completely consistent with the finite element simulation result of M = 5.9 kN·m. The aerodynamic coefficients show a linear relationship with wind speed, which conforms to the similarity law of fluid mechanics, verifying the reliability of the 1:20 scale model. When the wind speed is increased to 49 m/s and the wind direction is 0°, the support exhibits a typical failure mode: cracking of the weld between the bearing housing and the column, with a failure torque of 18.4 kN·m, which is 3.1 times the design load of 5.9 kN·m, meeting the IEC 61215 standard requirement of "safety factor ≥ 2.5" for typhoon areas.

2.2.4 Strength verification of key components

By comparing theoretical calculations, finite element simulations, and experimental tests, as shown in Table 3, it was found that the theoretical tensile stress of the bolt connection (28.1 MPa) differed from the experimental value of 29.3 MPa by 4.3%; the shear stress (111.2 MPa) differed from the experimental value of 115.6 MPa by 3.9%; the theoretical stress of the bearing housing assembly (196 MPa) differed from the finite element result of 205 MPa by 4.6%; and for the purlin, the maximum bending moment under a 60° wind direction was 4.2 kN·m, and the experimental deflection was 12.7 mm, which differed from the theoretical value of 13.5 mm by 5.9%.

Table 3 Comparison of Mechanical Response of Key Components

part	Theoretical value	Finite element value	Experimental values	Maximum error
Bolt tensile stress	28.1MPa	28.9MPa	29.3MPa	+4.3%
Bearing housing assembly stress	196MPa	205MPa	202MPa	+4.6%
Purlin deflection	13.5mm	13.1mm	12.7mm	-5.9%

2.2.5 Analysis of factors affecting wind stability

When the wind direction increases from 0° to 60°, the uplift wind load coefficient of the component increases from GCN1uptwist = -0.8 to -2.04, resulting in: corner support torque increasing from 5.5 kN·m to 8.3 kN·m (a 51% increase); bolt axial tensile force increasing from 8.8 kN to 13.2 kN (a 50% increase); and purlin mid-span bending moment increasing from 3.1 kN·m to 4.9 kN·m (a 58% increase).

Comparing the 5% and 10% turbulence intensity conditions, it was found that the root mean square acceleration of the support vibration increased from 0.8g to 1.3g (a 62.5% increase); the bolt alternating stress amplitude increased from 12 MPa to 18.5 MPa (a 54.2% increase); and the turbulence integral scale in the component wake region increased from 0.5m to 0.8m (a 60% increase).

3 Research on Optimization Design of Purlin Structure

3.1 Experimental protocol

3.1.1 Photovoltaic module support structure

The single-axis photovoltaic tracking bracket selected in this study achieves real-time tracking of the solar panels through single-axis rotation. Its typical structure consists of five core components. The rotary drive device is the "power core" of the tracking bracket, driving the main shaft to rotate via a motor, allowing the photovoltaic panels to rotate according to the solar azimuth/altitude angle. The main shaft is horizontally arranged, connecting the column and purlins. The panels are fixed to the main shaft via the purlins, and the entire structure rotates around the main shaft. The column is perpendicular to the ground, while the main shaft is horizontal.

3.1.2 Finite element model establishment

This study analyzes the influence of purlin thickness, U-shaped reinforcement parameters, and diagonal bracing structure on the wind resistance stability of a single-axis photovoltaic support system using finite element simulation. The structural design is optimized to address the local buckling problem of the purlin flange, and the economic efficiency and effectiveness of structural optimization and material upgrade schemes are compared. A purlin structure model of the single-axis photovoltaic support system is established using ANSYS, with core parameters shown in Table 5. Purlins and U-shaped reinforcements are modeled using Shell181 shell elements, and the mesh is generated using multi-region tetrahedral discretization with element sizes ≤10mm. The contact relationship is set as frictional contact between the purlin and the frame with a friction coefficient of 0.3. Bolted connections are simulated using RB2 rigid elements, and the main shaft is fixed at both ends. Load conditions include an upward force of 1200Pa and a downward force of 2700Pa. The baseline model uses Q355 steel with an elastic modulus of 210GPa and a yield strength of 355MPa. The optimized scheme using Q500 steel with a yield strength of 500MPa is adopted.

Table 4 Parameters of Main Components of the Model

Component	length（mm）	thickness（mm）
purlins	3830	1.5
U Type of	200	1.5

reinforcement		
External reinforcement	400	2
diagonal brace	750	2

3.2 Optimization analysis of structures with diagonal bracing

3.2.1 Purlin Thickness Optimization Analysis

While maintaining the cross-sectional geometry of the purlins, this paper selects three thicknesses—1.5mm, 1.8mm, and 2.0mm—as research objects to analyze their buckling response and stress distribution characteristics under upward loads. Simulation results show that as the purlin thickness gradually increases, its critical buckling stress significantly increases, especially the local instability at the flange is significantly improved. At a thickness of 1.5mm, the bottom of the purlin flange remains the dominant buckling region, and the maximum equivalent stress is close to the material's yield limit.

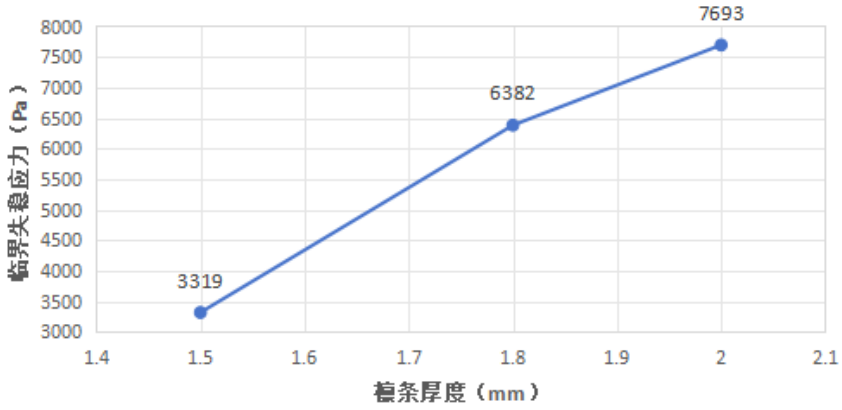

Figure 3. Relationship between purlin thickness and critical instability stress

3.2.2 U Optimization analysis of type reinforcement components

As a key component for improving the local stiffness of the flange, the U-shaped reinforcement has a significant impact on the stability performance of the purlin. To quantitatively assess its influence, this paper conducts simulation comparisons under different lengths of 200mm, 250mm, 300mm, and 370mm, and different placement positions from the purlin center of 0 to 120mm.

(1) Length Optimization

Analysis shows that as the length of the U-shaped reinforcement increases, its ability to improve the local buckling stress of the purlin exhibits a marginal decrease characteristic. When the length of the reinforcement exceeds 300mm, the increase in critical stress tends to stabilize, and further lengthening has no significant optimization effect. 200mm length: limited improvement effect, and obvious buckling of the flange still exists; 300mm length: the increase in critical stress is most significant, and the buckling area obviously spreads outward; 370mm length: after further lengthening, the optimization range tends to saturate, and the increase in structural weight is not

cost-effective.

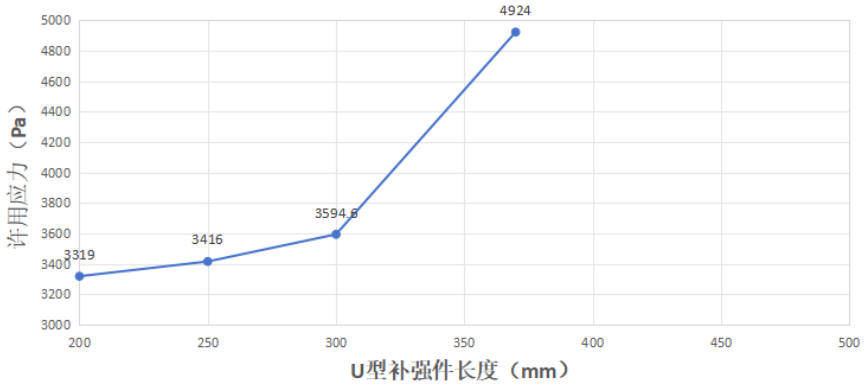

Figure 4. Relationship between the length of the U-shaped reinforcement and the allowable stress for local buckling instability.

（2）Location optimization

This study aims to further optimize the bracing structure by analyzing the impact of the positional variation of the U-shaped reinforcement on the buckling performance of the purlin while maintaining a reinforcement length of 300 mm. Simulations were conducted to compare different placements of the U-shaped reinforcement at distances from the purlin center, ranging from 0 to 120 mm. The experimental results are shown in the figure below. The simulation results indicate that excessive lateral compressive load on the flange is a significant factor causing local buckling failure of the purlin; the closer to the purlin center, the greater the internal force in the flange. The U-shaped reinforcement bears a larger share of the lateral load.

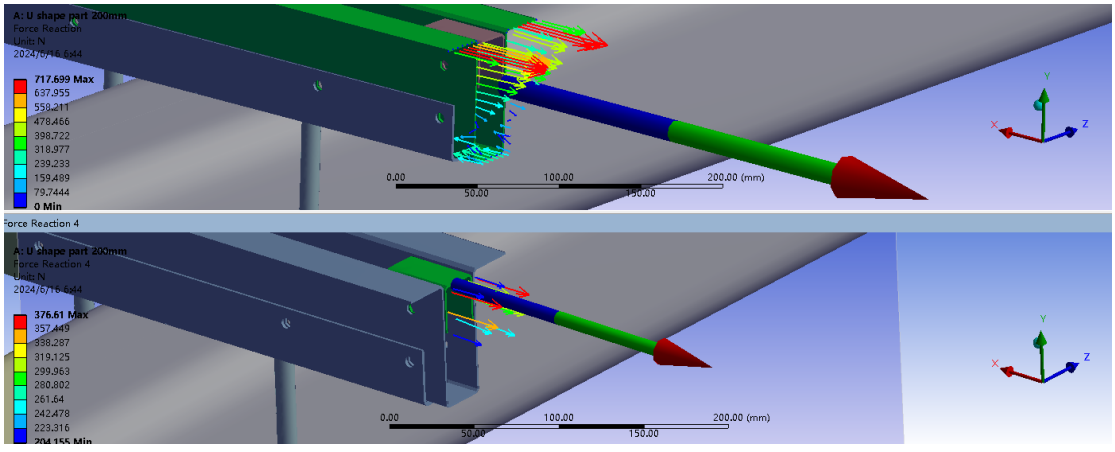

Figure 5. Finite element comparison of the stress response of the U-shaped reinforcement at 300mm.

While maintaining a reinforcement length of 300mm, the influence of its positional variation on purlin buckling performance was further analyzed. The results showed that when the reinforcement was placed within ±50mm~70mm of the purlin center, local flange stress concentration was significantly alleviated. Specifically, when the reinforcement was placed close to the center (within 50mm~70mm), the buckling modes tended to disperse, resulting in the most significant improvement in overall stiffness. When placed further away from the center, the

flange's internal force sharing capacity decreased, and the optimization effect was unsatisfactory. Further attempts to move it more than 120mm further away resulted in essentially no change in the structural buckling characteristic value, and the optimization effect of the reinforcement almost disappeared. Therefore, it is recommended that the length of the U-shaped reinforcement be controlled at around 300mm, and that it be preferentially placed within ±50~70mm of the purlin center to fully utilize its buckling-inhibiting effect.

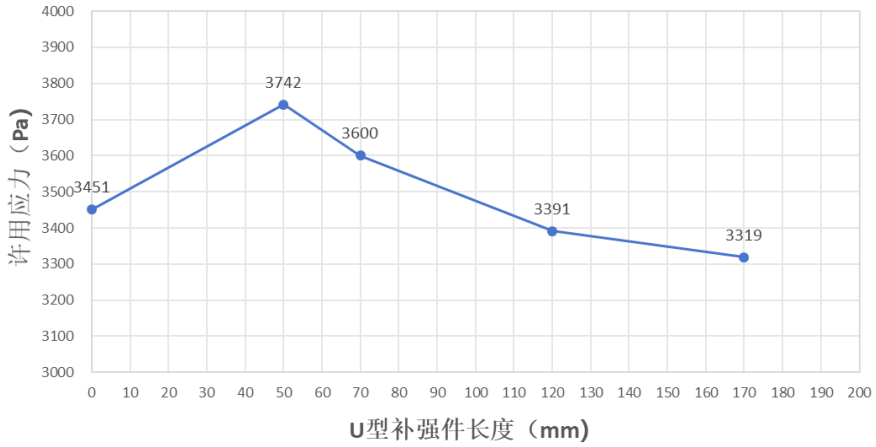

Figure 6. Relationship between the length of the U-shaped reinforcement and the allowable stress for local buckling instability.

3.2.3 Optimization analysis of diagonal bracing structure

As a crucial component supporting the overall stress path of the purlins, the angle, thickness, and arrangement of the bracing structure all affect the stability of the overall structure. This paper analyzes the impact of angle and thickness on the buckling behavior of the purlins.

(1) Optimization of Bracing Angle

Comparing multiple angle arrangements such as 5.2°, 7.2°, and 10.2°, the impact on overall stability under the same load is analyzed. The figure below shows that the 5.2° scheme currently used in the project exhibits good stability among various optimized parameters and is the optimal arrangement angle; a larger bracing angle of 10.2° will increase the slenderness ratio of the bracing members, which will reduce their stiffness and cause premature instability of the purlins; a smaller angle of 3.2° may not be feasible under the condition of limited component spacing. Therefore, the currently used 5.2° bracing angle achieves a good balance between structural efficiency and construction feasibility, and it is recommended to continue using it.

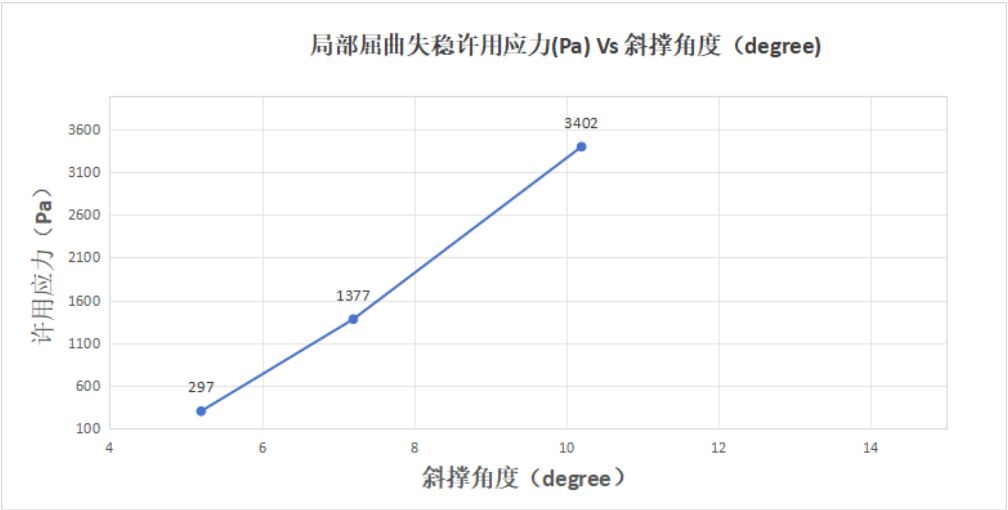

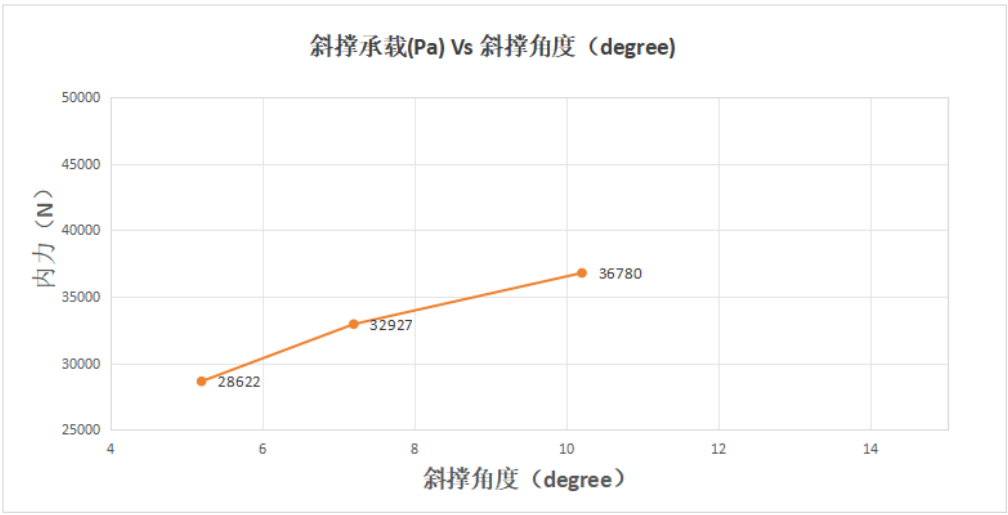

Figure 7 Comparison of the relationship between the brace angle, allowable stress for local buckling instability, and brace bearing capacity.

（2）Diagonal brace thickness optimization

Analyzing different brace thicknesses while keeping the brace angle constant, we found that the brace's role in the overall force flow transmission of the purlin becomes more significant with increasing thickness. When the thickness increases by approximately 30% from the current standard value, the purlin buckling mode changes significantly, with the first-order buckling mode shifting from overall brace instability to local instability at the component boundary, indicating improved overall stability. However, excessively thick braces may lead to increased costs and inconsistent deformation of connecting components. Therefore, it is recommended to appropriately increase the brace thickness in the design to improve the overall load-bearing capacity, while balancing structural cost and ease of construction.

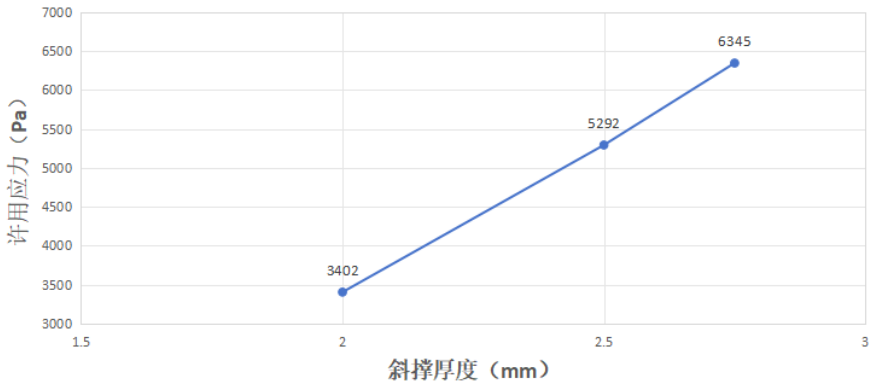

Figure 8. Relationship between brace thickness and allowable stress for local buckling instability

3.3 Optimization analysis of structures without diagonal bracing

Compared to structures with diagonal bracing, purlin structures without diagonal bracing are more prone to problems such as localized flange buckling and decreased overall stability under compression or uplift forces. Therefore, multi-parameter optimization is needed to compensate for their lack of support capacity. This paper uses the finite element method (FEM) simulation analysis to optimize the structural performance around key parameters such as purlin thickness increase and the length and position of U-shaped reinforcement members, in order to improve its critical buckling stress and overall safety margin.

3.3.1 Purlin Thickness Optimization Analysis

Comparing the buckling responses of unbraced purlin structures with thicknesses of 1.5mm, 1.8mm, 2.0mm, and 2.5mm under a -1200Pa uplift force, the results show that at a thickness of 1.5mm, significant buckling deformation occurs at the flange base, with local instability being the main failure mode; at a thickness of 2.0mm, the instability of the purlin flange is significantly reduced, and the structural stiffness is significantly improved; at a thickness of 2.5mm, local buckling of the purlin is basically eliminated in the first six buckling modes, and the structural load-bearing capacity is significantly enhanced.

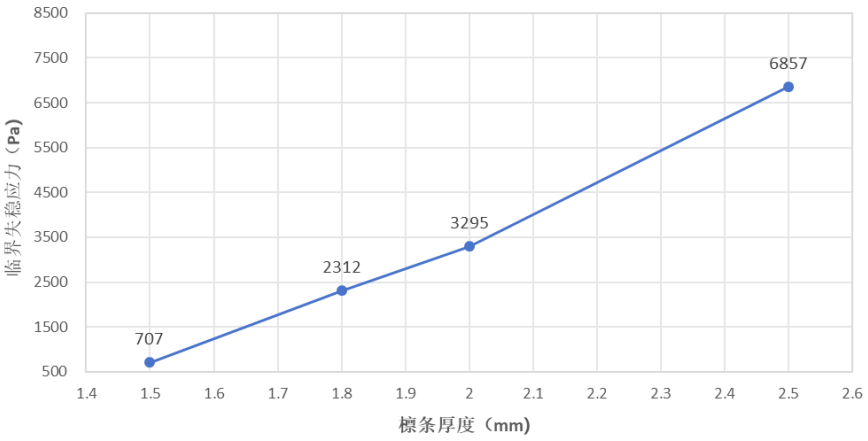

Figure 9. Relationship between purlin thickness and critical instability stress

Such optimizations demonstrate that even in the absence of diagonal bracing, adjusting the thickness

can effectively improve the instability resistance of the purlin structure. A design thickness of at least 2.0 mm is recommended to achieve safety redundancy control.。

3.3.2 Optimization analysis of the length of the U-shaped reinforcement

U-shaped reinforcements are an important measure to improve purlin flange stiffness, especially in the absence of diagonal bracing, where the load-bearing path is more concentrated and the effect is more significant. This section compares the structural response when the reinforcement length is 200mm, 250mm, 300mm, and 370mm. With a reinforcement length of 200mm, the stiffness is insufficient, only slightly improving the stress distribution in the central area; 250-300mm is the effective improvement range, especially at 300mm, where the buckling response in the middle of the flange is most alleviated; although a 370mm length provides greater stiffness, the increase in the critical buckling stress is no longer significant, and there is a risk of material waste and installation interference. Therefore, it is recommended to use 300mm long U-shaped reinforcements as the optimal configuration in actual engineering design, ensuring structural performance while also considering material utilization and construction efficiency.

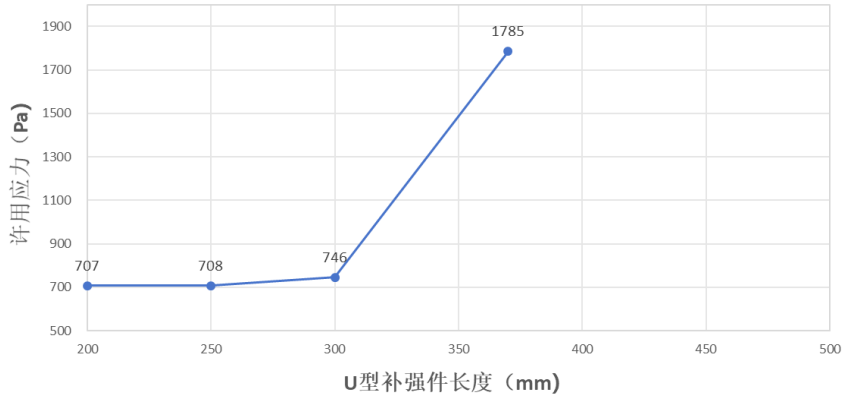

Figure 10 Relationship between the length of the U-shaped reinforcement and the allowable stress

3.3.3 Optimization analysis of the location of U-shaped reinforcement

To further leverage the role of U-shaped reinforcements in structural force flow, this paper conducts a comparative analysis of reinforcement placement at different locations, ranging from 0mm to ±120mm from the purlin center. U-shaped reinforcements placed within 50-70mm of the purlin center exhibit the best stability improvement effect; when placed more than 100mm from the center, the reinforcements fail to cover the maximum stress zone of the flange, and their optimization effect significantly diminishes. Modal analysis results also show that the buckling modes shift from local concentration to dispersion, with a substantial increase in critical stress. These conclusions indicate that precise placement of U-shaped reinforcements is crucial in the absence of diagonal bracing. It is recommended to position the reinforcement center within ±60mm of the center to maximize stiffness utilization and buckling delay capability.

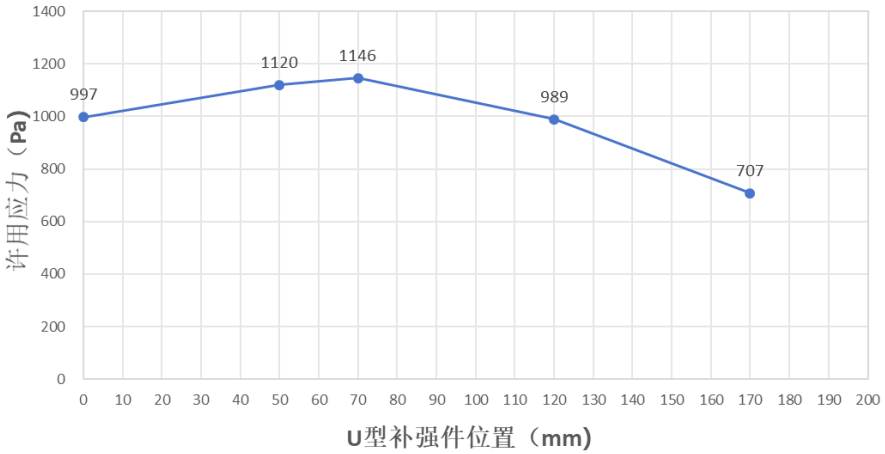

Figure 11 Relationship between the location of the U-shaped reinforcement and the allowable stress

3.4 Material strength comparison analysis

Besides optimizing purlin structural parameters such as thickness, bracing, and reinforcement, altering the yield strength of the material is also a common strategy to improve overall structural stability. Therefore, this paper, based on existing optimized structures, compares and analyzes the instability response characteristics of purlin structures under a 2700Pa pressure condition using materials with different yield strengths, Q235 and Q500, aiming to clarify the actual impact of material strength on buckling performance.

3.4.1 Finite element simulation analysis

Equivalent models were established for two steel materials, Q235 (yield strength 420 MPa) and Q500 (yield strength 500 MPa), and the simulated first-order buckling eigenvalues of the structures were both 1.264. This result indicates that increasing the material's yield strength has minimal impact on the structural buckling eigenvalues; the local buckling instability mode of the structure still occurs in the region connecting the purlin flange and the brace; and the critical buckling load is mainly constrained by geometric properties and boundary conditions, rather than the material strength itself.

3.4.2 Theoretical verification analysis

To further explore the role of material strength in the buckling performance of purlin structures, this paper introduces two classical buckling theory models: Euler's overall buckling theory and empirical formulas for local buckling. For slender compression members (such as long purlins or braces), overall buckling can be predicted by Euler's theory, and the formula for calculating the critical buckling load is as follows：

$$P_{cr} = \frac{\pi^2 EI}{(KL)^2} \quad (4)$$

The corresponding critical buckling stress is:

$$\sigma_{cr} = \frac{P_{cr}}{A} = \frac{\pi^2 E}{\left(\frac{KL}{r}\right)^2} \quad (5)$$

In the formula, Pcr is the critical buckling load in N; σcr is the critical buckling stress in Pa; E is the elastic modulus, usually taken as 2.06×10^{11} Pa for steel; I is the moment of inertia of the section in m^4; A is the cross-sectional area in m^2; L is the calculated length of the member in m; and K is the length factor, which depends on the boundary conditions. The engineering criterion is that if σcr > fy, the member yields first; if σcr < fy, buckling instability occurs first. For plate members such as flanges or webs, especially in thin-walled purlin structures, local buckling is the main failure mode. Its critical stress can be given by the following empirical formula.

：

$$\sigma_{cr} = k \cdot \frac{\pi^2 E}{12(1-\nu^2)} \cdot \left(\frac{t}{b}\right)^2 \quad (6)$$

In the formula, σcr is the critical local buckling stress in Pa; k is the buckling coefficient, which depends on the boundary support conditions; E is the elastic modulus in Pa; ν is Poisson's ratio, usually taken as 0.3 for steel; t is the plate thickness in meters; b is the width of the free edge of the plate in meters. Typically, k ≈ 0.425, and when the boundary is fully fixed, k can reach 4.0~6.9. When σcr > fy, fy is taken as the actual buckling control stress; when σcr < fy, σcr is taken as the design limit.

From the above formula, it can be seen that the main control parameters for overall buckling are the slenderness ratio and support conditions. The main control parameters for local buckling are the plate thickness ratio, boundary support, and elastic modulus. The analysis results of this study show that although replacing the steel material with high-strength Q500 increases the yield strength fy, its effect on improving σcr is limited. If the structural geometric parameters are not optimized simultaneously, the structure may still preferentially experience instability. Therefore, optimizing structural parameters is more effective than material replacement in improving the buckling bearing capacity.

4 discuss

4. 1. Comparison of the benefits of structural parameter optimization and material upgrading

The above research results demonstrate that structural parameter optimization has a more direct and significant effect on improving purlin stability. Taking purlin thickness as an example, increasing it from 1.5mm to 2.5mm significantly enhances its critical buckling bearing capacity, and the buckling mode shifts, with the instability characteristic changing from local flange buckling to an overall response at the boundary constraint. This change not only improves the structure's safety margin but also enhances the stability of the stress path.

In contrast, the stability improvement obtained solely by replacing the steel with high-strength Q500 is relatively limited. Simulation results show that even with a yield strength increase to 500MPa, the first-order buckling characteristic value of the structure changes only slightly, and buckling still preferentially occurs in the purlin flange region, indicating that geometric characteristics remain the dominant factor controlling local buckling. Therefore, considering both economic efficiency and engineering feasibility, prioritizing the optimization of structural forms such as section thickness, reinforcement elements, and their arrangement can significantly improve instability resistance while controlling material usage, thus possessing greater practical application value.

4.2 Differences and Synergies in Optimization Strategies for Structures with and without Bracing

The optimization paths for purlin structures with and without diagonal bracing differ significantly when addressing stability challenges under high wind conditions. Structures with diagonal bracing utilize diagonal support members to form a stable triangular force flow system, exhibiting strong overall stability and easily dispersing local stresses. Optimization for this type of structure focuses on controlling the angle and thickness of the diagonal bracing, and reducing component dimensions to decrease material consumption while maintaining overall stiffness.

Structures without diagonal bracing, lacking diagonal support, have a longer overall force path, significantly increasing the risk of local buckling. Therefore, optimization for this type focuses on compensating for the lack of constraint by increasing purlin thickness and introducing U-shaped reinforcements. Studies show that placing reinforcements within 50 to 70 mm of the purlin center can effectively delay local instability and enhance the structure's compressive strength. It is worth

noting that in certain practical applications, the two types of structures may coexist or be used alternately. For example, using a brace-less scheme in areas with limited component placement, while installing diagonal bracing members in boundary areas or key stress zones, can achieve a balance between system stability and space utilization. Therefore, exploring a combined optimization design strategy for the two structural forms is expected to further improve the stability margin of the overall support system under high wind conditions.

4.3 Optimization window for diagonal bracing structural parameters

As a key stability support element, the selection of parameters for the diagonal bracing structure directly affects the wind resistance and construction efficiency of the support system. This study found that the diagonal bracing angle used in the current project, 5.2°, exhibited good structural stability under various load conditions. While larger angles can shorten the force path, they significantly increase the slenderness ratio of the members, reducing their stiffness and potentially inducing overall instability; smaller angles, on the other hand, are difficult to implement effectively due to limited construction space.

Regarding thickness, as the diagonal bracing increases by approximately 30% from the standard value, the overall purlin buckling mode is significantly optimized, indicating that increasing thickness can effectively enhance overall stability within a certain range. However, when the thickness is further increased, the resulting stiffness increase tends to saturate, accompanied by a significant increase in material costs and construction connection difficulty. Therefore, there is a clear parameter window for optimizing the diagonal bracing structure. It is recommended that the angle be controlled at around 5 degrees and the thickness between 2-2.5 mm to balance the comprehensive needs of structural performance, economic cost, and on-site construction.

Furthermore, the placement of the diagonal bracing members and the connection method of the nodes also have a significant impact on stability. Future research could further incorporate practical engineering constraints to conduct multi-objective optimization design of the bracing system, exploring the optimal configuration path of "minimum material consumption and maximum stability".

5 conclusion

This paper takes a photovoltaic tracking bracket in a high-wind area as the research object, and constructs a multi-scale analysis system of "theoretical modeling - finite element analysis - wind tunnel experiment" to systematically study the structural mechanical properties and wind resistance stability under extreme wind loads. A wind load model incorporating the tilt angle-wind direction coupling effect was established through theoretical derivation. The measured wind pressure

coefficient Cp ranged from -3.4 to 1.852, with an error of ≤5.9% compared to wind tunnel experimental data, verifying the accuracy of the model. The combination of finite element simulation and wind tunnel experiments revealed the stress distribution law for bolt connection tensile stress of 28.1 MPa (utilization rate 0.062) and bearing seat combined stress of 196 MPa (utilization rate 0.552). Under extreme conditions, the bracket's torsional failure threshold reached 18.4 kN·m. Experiments show that turbulence intensity increases the alternating stress of bolts by 54.2%, necessitating the inclusion of the fatigue effect of pulsating wind in the design. To address the structural stability and local buckling control of purlins under high wind conditions, this paper conducts a systematic parametric optimization study based on the finite element method (FEM). Taking two typical purlin structures—one with bracing and one without—as examples, FEM models are constructed under two typical working conditions: uplift and downforce. The buckling response and instability characteristics are analyzed, and structural optimization is carried out by considering factors such as thickness, reinforcement, and bracing arrangement. Furthermore, the role of high-strength steel Q500 in improving stability is evaluated. Experiments show that purlin thickness is the primary factor affecting structural stability. In both braced and unbraced structures, increasing the purlin thickness from 1.5 mm to 2.5 mm significantly increases the critical buckling stress and effectively alters the buckling mode, shifting local instability from the flange to the boundary connection region, resulting in a simultaneous improvement in structural stiffness and load-bearing capacity. U-shaped reinforcement plays a significant role in controlling local buckling. When the reinforcement is 300mm long and positioned within a purlin center area of ±50~70mm, it can significantly distribute the lateral pressure on the flange and effectively delay local buckling. This measure is particularly crucial in structures without diagonal bracing; the angle and thickness of the diagonal bracing have a significant impact on overall stability. Under downforce, the combination of a diagonal bracing angle of 5.2° and a thickness of 2.0~2.5mm exhibits optimal structural performance. The current diagonal bracing placement is already reasonable and requires no further adjustment; structural optimization is superior to material replacement strategies. While replacing with high-strength steel (Q500) increases the yield strength, it has limited effect on improving the critical stress at local buckling; however, by jointly optimizing geometric parameters such as thickness, reinforcement, and diagonal bracing, overall stability can be significantly improved, with better results in controlling instability and failure, and also better economic efficiency.

References

[1] He Xing'an. Research on the application of electrical automation technology in solar photovoltaic power generation grid-connected system [J]. Urban Construction Theory Research (Electronic Edition), 2025, (11): 1-3.

[2] Li Xiaohong. Supply and demand sides work together to promote the high-quality development of photovoltaic industry [N]. 2025-04-07.

[3] Wang Li, Song Zihua, Li Jiadong, et al. Research on the optimal angle calculation method of daytime adjustable single-axis photovoltaic bracket [J]. China Equipment Engineering, 2025, (08): 148-52.

[4] H. A E, A. F O. Thermal control of crystalline silicon photovoltaic (c-Si PV) module using Docosane phase change material (PCM) for improved performance [J]. Solar Energy, 2022, 234: 203-21.

[5] Zhang Yifan. Research on wind load characteristics and wind vibration response of large span photovoltaic tracking bracket [D], 2024.

[6] Wang Long, Wang Yunxia, Chen Jianfei, et al. Lightweight optimization design of support frame for photovoltaic panel cleaning robot [J]. Mechanical Design and Research, 2018, 34(04): 182-5.

[7] GILIO F H, VIEIRA JR L C, MALITE M. Stability and moment-rotation behavior of cold-formed steel purlins with sleeved bolted connection [J]. Engineering Structures, 2018, 171: 658-72.

[8] ZHAO C, YANG J, WANG F, et al. Rotational stiffness of cold-formed steel roof purlin–sheeting connections [J]. Engineering structures, 2014, 59: 284-97.

[9] LIANG X, HU L, WANG Y, et al. Analysis of single-span and multi-span continuous steel purlin beams reinforced with [10] Wang Weiyong, Gao Minglong. Experimental study on the effect of tensile rate on high-temperature strength of high-strength Q690 steel [J]. Journal of Southeast University (Natural Science Edition): 1-15.

[11] BAI F, YANG N, ZHANG H, et al. A modified direct strength method for nonlinear twisting model of simply-supported C-section purlins [J]. Journal of Constructional Steel Research, 2018, 150: 384-91.

[12] YOSSEF N, ELBOGHDADY A, EL-BOGHDADI M, et al. Synthetic SN Curve of Steel Beams with Web Opening [J]. Arabian Journal for Science and Engineering, 2023, 48(4): 5525-48.

[13] PANG Z, CHEN R, CAO Y. Performance analysis and optimization for static mixer of SCR denitration system under different arrangements [J]. Energies, 2022, 15(23): 8977.

[14] SHAO Y-B, MOHAMED H S, HASSANEIN M F, et al. Static strength of square T-joints

reinforced with collar-plates under axial compression or in-plane bending [J]. International Journal of Civil Engineering, 2020, 18: 1009-23.

[15] PAŘENICA P, KREJSA M, BROŽOVSKý J, et al. Verification of Numerical Models of High Thin-Walled Cold-Formed Steel Purlins [J]. Materials, 2024, 17(17): 4392.